J Incl Phenom Macrocycl Chem (2012) 74:117–127
DOI 10.1007/s10847-011-0090-8

ORIGINAL ARTICLE

Transition metal complexes enslaved in the supercages of zeolite-Y: DFT investigation and catalytic significance

Chetan K. Modi · Parthiv M. Trivedi · Sanjeev K. Gupta · Prafulla K. Jha

Received: 21 September 2011 / Accepted: 17 November 2011 / Published online: 27 November 2011

Abstract A series of zeolite-Y encapsulated hybrid catalysts, [M(STCH)·xH_2O]-Y have been prepared by encapsulating Schiff base complexes [where M = Mn(II), Fe(II), Co(II), Ni(II); ($x = 3$) and Cu(II); ($x = 1$); H_2STCH = salicylaldehyde thiophene-2-carboxylic hydrazone] in zeolite-Y matrix by flexible ligand method. These hybrid materials have been characterized by various physicochemical techniques such as ICP-OES, elemental analyses, (FT-IR and electronic) spectral studies, BET, scanning electron micrographs, thermal analysis and X-ray powder diffraction patterns. X-ray powder diffraction analysis reveals that the structural integrity of the mother zeolite in the hybrid material remained intact upon immobilization of the complex. Density functional theory is employed to calculate the relaxed structure, bond angle, bond distance, dihedral angle, difference of highest occupied molecular orbital and lowest unoccupied molecular orbital energies gap and electronic density of states of ligand and their neat transition metal complexes. The hybrid materials are active catalysts for the hydroxylation of phenol using hydrogen peroxide (30% H_2O_2) as an oxidant in order to selectively synthesize catechol or hydroquinone, amongst them [Cu(STCH)·H_2O]-Y shown the highest % of selectivity towards catechol (81.3%).

C. K. Modi (✉) · P. M. Trivedi
Department of Chemistry, Bhavnagar University, Bhavnagar 364 002, Gujarat, India
e-mail: chetank.modi1@gmail.com

S. K. Gupta · P. K. Jha
Computational Condensed Material Physics Laboratory, Department of Physics, Bhavnagar University, Bhavnagar 364 022, Gujarat, India

Keywords Zeolite-Y encapsulated hybrid materials · Transition metal complexes · DFT · Catalytic hydroxylation of phenol

Introduction

In recent years, to design transition metal active centers on molecular sieves have attracted considerable attentions as the novel catalysts, owing to which possess the advantages of both homogeneous catalysis as the metal ion in the solution and heterogeneous catalysis as the molecular sieve in the polyphase system. These nanoporous molecular sieves possess suitable surface area and uniform nanoporous channels, which are advantageous characteristics of a catalytic support.

Nanopores encapsulated hybrid materials are widely used as heterogeneous catalysts in various industrially important reactions. They form the basis of new eco-friendly techniques, involving inexpensive, most effective and environmentally greener ways for carrying out various oxidative transformation reactions such as oxidation of phenol, cyclohexane, cyclohexene, benzyl alcohol, ethylbenzene, epoxidation of styrene and hydroxylation of benzene [1–8]. Hydroxylation of phenol to catechol and hydroquinone is an industrially important reaction. Several research groups have developed different catalytic methods for hydroxylation of phenol to catechol and hydroquinone, in which TS-1 and TS-2 was commercially employed for this purpose [9, 10]. Maurya et al. have synthesized encapsulated oxovanadium (IV) and copper (II) complexes with amino acid as well as Schiff base ligands in the zeolite-Y and studied their catalytic properties for the oxidation of unsaturated hydrocarbons [1, 11]. Neves et al. have presented in situ encapsulation of selected transition

metal complexes [Ni(II), Cu(II) and Zn(II)] as a guest with 1-(2-pyridylazo)-2-naphthol (PAN) ligand in supercages of zeolite-Y (host) using FLM and their results indicated that complexes were encapsulated in the supercages of zeolite-Y. The choice of any specific method is being dictated by the size of ligands relative to the free diameter of zeolite-Y channels. Complexes or ligands that are smaller than the channels can be adsorbed from a solution phase into the zeolite-Y, or they can be synthesized via diffusion of the ligand by the flexible ligand method into a metal-exchanged zeolite-Y [12]. Further some studied on the zeolite-encaged metal complexes extent to the enzymes, where the catalytic center might be a transition metal ion and the protein provides the stability and steric constraints. Vishwanathan and co-workers [13] reported density functional calculations (DFT) studies and evaluated redox properties of neat and encapsulated Mn–Qn complexes by cyclic voltammetery. The structural elucidation of Schiff base ligand (H_2STCH) and their metal complexes is fundamental to understand host–guest interaction. Sawabe et al. [14] have performed density functional calculation and observed that hydrogen promotion effect for the selective catalytic reduction of NO_x over Ag-MFI zeolite and nature of bond between Ag and MFI is ionic. Density functional calculation can play a crucial role to clarify fundamental aspects concerning the chemistry of structural parameter, complex formation, host–guest interaction and different allied properties like highest occupied molecular orbital (HOMO), lowest unoccupied molecular orbital (LUMO) and formation energy. The scattered study such as Møller–Plesset perturbation theory (MP2, MP3 or MP4), molecular dynamics (MD) [15], semi-empirical quantum mechanics (QM) [16] methods and Hartree–Fock method [17] were performed to study the complex formation. However, due to large size in molecule, few study reported using first principles with appropriated plane wave basis set and ultrasoft pseudopotential method [18, 19].

The objective of the present investigation is to develop a catalytic system for liquid-phase hydroxylation of phenol with 30% H_2O_2 to give catechol as a major product and hydroquinone as minor product. Considering the effect of solvent, amount of catalyst and effect of temperature, an optimal reaction condition has been optimized to get maximum hydroxylation. With this view herein we report the preparation, characterization and catalytic activity of novel zeolite-Y encapsulated hybrid materials containing salicylaldehyde thiophene-2-carboxylic hydrazone ligand (H_2STCH) in combination with DFT. Results of DFT for Schiff base ligand (H_2STCH), [Cu(STCH)·H_2O] and [Mn(STCH)·3H_2O] were used to explore the energetics of the metal–ligand interactions and the possibility for the compound to adopt different conformations. The Schiff base ligand is shown in Scheme 1.

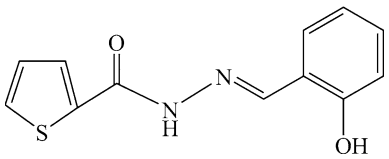

Scheme 1 The Schiff base ligand (H_2STCH) under study

Experimental

Materials and methods

All chemicals and solvents used were of AR grade and used without further purification. Salicylaldehyde was purchased from Loba Chemie (India). Thiophene-2-carboxylic acid was obtained from spectrochem (India). 30% H_2O_2 purchased from Rankem (India). The Schiff base ligand (H_2STCH) was synthesized by the condensation of salicylaldehyde with thiophene-2-carboxylic acid hydrazide according to reported procedure [20]. Sodium form of zeolite-Y (Si/Al = 2.60) was procured from Hi-media, India. It was dried at 400 °C for 6 h before being used as host material for encapsulation of complexes.

Instrumentation

The Si, Al, Na and transition metal ions in the encapsulated hybrid materials were determined by ICP-OES (Model: PerkinElmer optima 2000 DV). Carbon, hydrogen and nitrogen were analyzed with a Perkin Elmer, USA 2400-II CHN analyzer. IR spectra of encapsulated hybrid materials were recorded on a Thermo Nicolet IR200 FT-IR spectrometer in KBr. UV–Visible spectra were recorded on Spectrophotometer Make/model Varian Cary 500, Shimadzu. The crystallinity of compounds was ensured by XRD using a Bruker AXS D_8 Advance X-ray powder diffractometer with a Cu Kα target. The surface area of encapsulated hybrid materials was measured by multipoint BET method using ASAP 2010, micrometrics surface area analyzer. A simultaneous TGA/DTA of the encapsulated hybrid materials has been obtained by Perkin Elmer Diamond TG–DTA Instrument. The experiments were performed in N_2 atmosphere at a heating rate 10 °C min^{-1} in the temperature range 50–800 °C, using Al_2O_3 crucible. The scanning electron micrographs of encapsulated hybrid materials were recorded using a SEM instrument (Model: LEO 1430 VP). The compounds were coated with a thin film of gold before recording the SEM to protect surface material from thermal damage by the electron beam.

Preparation of M^{II}-Y (metal exchanged zeolite-Y)

A series of zeolite-encapsulated hybrid catalysts have been prepared by flexible ligand method (FLM) as shown in

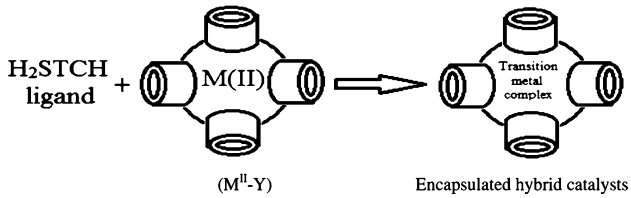

Scheme 2 Synthesis of zeolite-Y encapsulated hybrid catalysts

Scheme 2. An amount of 5.0 g of zeolite-Y was suspended in 300 mL of deionized water containing 12 m mol metal salt ($Mn(CH_3COO)_2{\cdot}4H_2O$, $FeSO_4{\cdot}7H_2O$, $Co(CH_3COO)_2{\cdot}4H_2O$, $Ni(CH_3COO)_2{\cdot}4H_2O$ and $Cu(CH_3COO)_2{\cdot}H_2O$, respectively) with constant stirring. The reaction mixture was then heated at 90 °C for 24 h. The solid was filtered, washed with hot deionized water until the filtrate was free from any metal ion content, and dried for 15 h at 150 °C in air.

Preparation of zeolite encapsulated hybrid catalysts

In the next step, 1.0 g of M^{II}-Y (calcinated at 450 °C in a muffle furnace for 4 h prior to use) was uniformly mixed with an excessive amount of H_2STCH ligand ($n_{ligand}/n_{metal} = 3$) in ethanol, and sealed into a round bottom flask. The reaction mixture was refluxed ($\sim$24 h) in an oil-bath with stirring. The resulting material was taken out, followed by Soxhlet extraction with ethanol, acetone and finally with acetonitrile (6 h) to remove uncomplexed ligand and the complex adsorbed on the exterior surface of zeolite-Y. The extracted sample was ion-exchanged with 0.01 M NaCl aqueous solution for 24 h to remove uncoordinated M^{II} ions, followed by washing with deionized water until no Cl^- ion could be detected with $AgNO_3$ solution. The final product was collected and dried at 120 °C.

Computational discussion

The electronic structures of the atoms are as follows: $C[He]2s^22p^2$; $N[He]2s^22p^3$; $O[He]2s^22p^4$; $S[Ne]3s^23p^4$; $Mn[Ar]3d^54s^1$ and $Cu[Ar]3d^{10}4s^1$. The geometry of all the structures considered in this work has been optimized using plane wave pseudopotential implemented in QUANTUM ESPRESSO [21–24]. The exchange and correlation effects were treated using Perdew–Burke–Ernzerhof generalized gradient potential approximation (PBE-GGA) [25]. The energy cutoff was set to 40 Ryd, and the self consistent calculation were considered to be converged using the conjugate-gradient algorithm until the absolute value of the forces on unconstrained atoms was less than 0.03 eV $Å^2$ and up to a precision of 10^{-4} eV in total energy difference. The Brillouin zone sampling was restricted to the gamma point [26]. Marzari–Vanderbilt [27] Gaussian smearing with a width of 0.05 Ryd was used to accelerate convergence of the total-energy calculations. For density of states calculations we increased the sampling of the Brillouin zone.

Catalytic hydroxylation of phenol

The catalytic hydroxylation of phenol was undertaken in a two-necked 50 mL round bottomed flask. In a typical reaction, 30 m mol of the substrate was taken in 2 mL of acetonitrile, add 45 mg of the catalyst to it and equilibrated at 80 °C in an oil-bath. 45 m mol of 30% H_2O_2 solution (phenol/H_2O_2 molar ratio, 1:1.5) was added to this with continuous stirring for 6 h. The products were collected at different time intervals and were identified and quantified by GC.

Results and discussion

The analytical data of host zeolites and zeolite-Y encapsulated hybrid materials are given in Table 1. The neat zeolite-Y has a Si–Al ratio is 2.60, indicating no dealumination during the encapsulation by FLM. Surface area and pore volume values estimated by nitrogen adsorption isotherms at relative pressures (p/p_0) given in Table 2. The results evaluated drastic reduction of surface area and pore volume of zeolite on encapsulation of metal complexes, which indicate the presence of complexes inside the nanocavity of zeolite-Y [28, 29].

Scanning electron micrographs (SEMs) of [Cu(STCH)·H_2O]-Y recorded before and after Soxhlet extraction are shown in Fig. 1, which shows well defined crystals after Soxhlet extraction, no surface complexes are seen and the particle boundaries on the external surface of zeolite are clearly distinguishable. During the process of encapsulation and Soxhlet extraction, the framework of the zeolite-Y was not damaged. These micrographs reveal the efficiency of purification procedure to effect complete removal of extraneous complexes, leading to the presence of well-defined encapsulation in the cavity.

X-ray powder diffraction measurements have been done for encapsulated hybrid materials, metal exchanged zeolite-Y and neat Na-Y. Comparison of XRD patterns of encapsulated hybrid materials and metal exchanged zeolite-Y with the standard patterns of Na-Y showed almost no significant changes in peak positions of the diffraction lines (Fig. 2). However, a little change occurred in the relative peak intensities of (3 3 1), (3 1 1) and (2 2 0) upon introducing the metal ions or complexes. In neat Na-Y intensity values were found in the order $I_{331} > I_{220} > I_{311}$. Upon exchanging the metal or after the encapsulation

Table 1 Analytical and physical data of compounds

Sr. no.	Compound	Color	Elements % found							
			%C	%H	%N	%M	%Si	%Al	%Na	Si/Al
1	Na-Y	White	–	–	–	–	17.16	6.60	9.86	2.60
2	Mn^{II}-Y	Dull white	–	–	–	2.40	17.08	6.56	5.68	2.60
3	[Mn(STCH)·3H_2O]-Y	Yellow	0.95	0.38	0.19	2.15	16.91	6.50	7.45	2.60
4	Fe^{II}-Y	Beige	–	–	–	5.33	16.85	6.48	6.25	2.60
5	[Fe(STCH)·3H_2O]-Y	Light orange	1.34	0.82	0.26	2.89	16.39	6.30	6.85	2.60
6	Co^{II}-Y	Light pink	–	–	–	3.53	16.80	6.46	4.87	2.60
7	[Co(STCH)·3H_2O]-Y	Yellow	1.22	0.53	0.24	1.75	16.57	6.37	5.30	2.60
8	Ni^{II}-Y	Light green	–	–	–	3.62	16.98	6.53	3.92	2.60
9	[Ni(STCH)·3H_2O]-Y	Light yellow	1.15	0.49	0.23	1.83	16.64	6.40	5.34	2.60
10	Cu^{II}-Y	Pale blue-green	–	–	–	4.71	16.90	6.50	7.01	2.60
11	[Cu(STCH)·H_2O]-Y	Dull green	1.10	0.64	0.23	1.30	16.77	6.45	6.90	2.60

Table 2 Surface area and pore volume data of compounds

Compound	Surface area (m^2/g)	Pore volume (cc/g)[a]
Na-Y	548	0.32
Mn^{II}-Y	538	0.29
[Mn(STCH)·3H_2O]-Y	385	0.20
Fe^{II}-Y	530	0.28
[Fe(STCH)·3H_2O]-Y	380	0.19
Co^{II}-Y	530	0.30
[Co(STCH)·3H_2O]-Y	372	0.21
Ni^{II}-Y	527	0.30
[Ni(STCH)·3H_2O]-Y	376	0.20
Cu^{II}-Y	534	0.31
[Cu(STCH)·H_2O]-Y	397	0.23

[a] Calculated by the BJH-method

process affects the relative peak intensities of (3 1 1) and (2 2 0) peaks, the intensity being in the order $I_{331} > I_{311} > I_{220}$. This indicates that the crystallinity of the zeolitic matrix remained intact upon encapsulation of the metal complex. The analysis of SEMs image also supports the assertion that all the modified zeolite has retained the crystallinity of the zeolite-Y.

The IR spectral data of ligand H_2STCH and their encapsulated hybrid materials are shown in Table 3. On comparing the main IR frequencies of encapsulated hybrid materials with that of H_2STCH ligand, the following results were found. The ν_{str}(C–O) of the ligand shifted from 1266 to ~1271 cm^{-1} in all the encapsulated hybrid materials. The H_2STCH ligand exhibits a strong band at 1596 cm^{-1} due to azomethine (C=N) group. This band is shifted to lower frequency region upon complexation with the metal by 15–30 cm^{-1} [30, 31], suggesting coordination via the

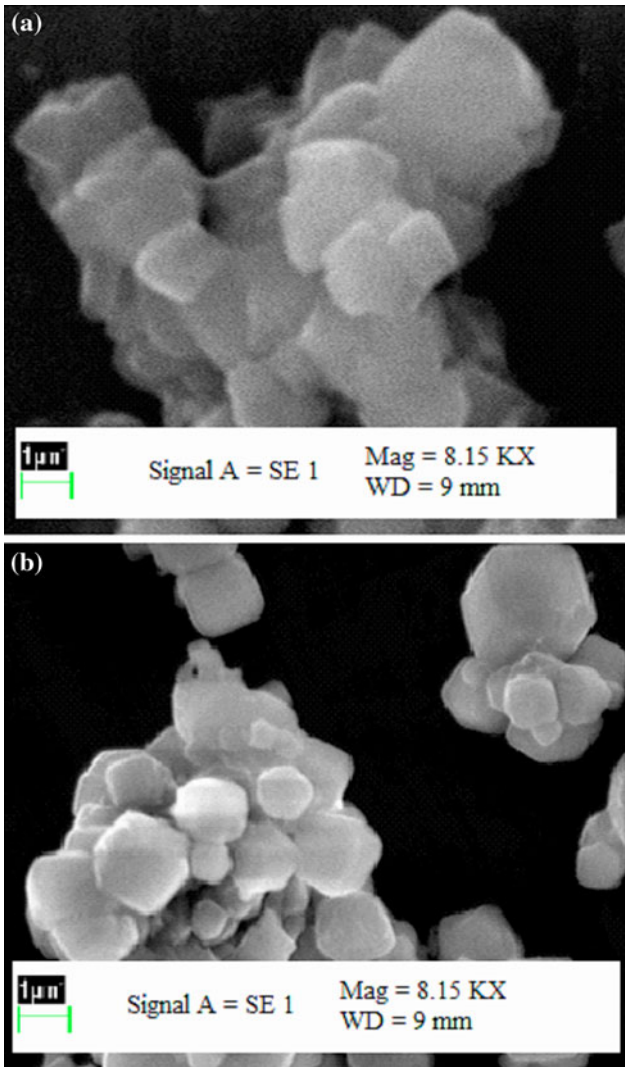

Fig. 1 SEM images of [Cu(STCH)·H_2O]-Y **a** before and **b** after soxhlet extraction

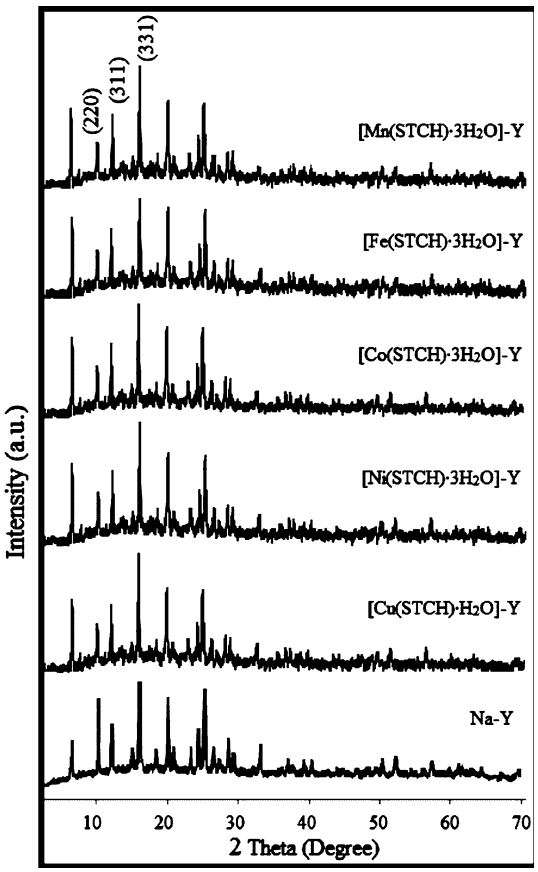

Fig. 2 XRD patterns of Na-Y and its modified zeolites

azomethine group in the encapsulated hybrid materials (M←N). In the investigated encapsulated hybrid materials, the broad band observed at ~3400 cm^{-1} and other very weak bands 830–860, 690–710 cm^{-1} are attributed to –OH stretching, rocking and wagging vibrations, respectively, due to the presence of water molecules [32]. It is evident that framework vibration bands of Na-Y dominate the spectra below 1200 cm^{-1} for all encapsulated hybrid materials. The bands at 572, 730 and 1029 cm^{-1} are attributed to T–O (structure-sensitive band) double ring, symmetric stretching and asymmetric stretching vibrations, respectively [33]. No shift was observed upon encapsulation of transition metal complexes; further substantiating that zeolite framework remains unchanged.

The electronic spectral bands of H_2STCH Schiff base ligand and their encapsulated hybrid materials are discussed. The H_2STCH ligand exhibits three bands at 210, 349 and 389 nm due to ILCT (intra ligand charge transfer transition), $\pi \rightarrow \pi^*$ and $n \rightarrow \pi^*$ transitions, respectively. In the electronic spectrum of encapsulated hybrid material [Mn(STCH)·$3H_2O$]-Y, the characteristic bands appear at 658, 448 and 321 nm are assignable to $^6A_{1g} \rightarrow {}^4T_{1g}$ (ν_1), $^6A_{1g} \rightarrow {}^4T_{2g}$ (ν_2) and $^6A_{1g} \rightarrow {}^4A_{1g}$, ^4E_g (ν_3) transitions, of a distorted octahedral geometry around the metal ion respectively [34]. The electronic spectrum of [Fe(STCH)·$3H_2O$]-Y exhibits band at 294 nm may be assignable to MLCT transition. [Co(STCH)·$3H_2O$]-Y displays four bands at 713, 323, 255 and 211 nm are attributed to $^4T_{1g}(F) \rightarrow {}^4A_{2g}(F)$, $^4T_{1g}(F) \rightarrow {}^4T_{1g}(P)$, MLCT and ILCT transitions of an octahedral geometry around the metal ion, respectively. The absorption spectrum of [Ni(STCH)·$3H_2O$]-Y exhibits two bands at 676 and 238 nm may be attributed to $^3A_{2g} \rightarrow {}^3T_{1g}(P)$ (ν_3) and $^3A_{2g} \rightarrow {}^3T_{1g}(F)$ (ν_2) transitions, respectively [35]. The electronic spectra of [Cu(STCH)·H_2O]-Y consists of shoulders at ~353 nm and a broad shoulder around 460 nm, which can be assigned to the $d_{xz,yz} \rightarrow d_{xy}$ and $d_{x^2-y^2} \rightarrow d_{xy}$ transitions, while other ligand bands appear at 253 and 210 nm, which may be assignable for tetrahedrally distorted (D_{2h}) mononuclear copper(II) complexes [36].

The thermogravimetric analysis data along with the percentage weight loss at different steps and their possible assignments are presented in Table 4. The TG–DTA curves of one of the representative catalyst, [Mn(STCH)·$3H_2O$]-Y is given in Fig. 3. The thermal decomposition of the catalyst [Mn(STCH)·$3H_2O$]-Y undergoes in two stages. The weight loss (16.6%) in the first step starts shortly after increasing the temperature and continues until the loss of intrazeolite water and coordinated water molecules from the species. This dehydration process is accompanied by endothermic effect at 101 °C in DTA curve [37]. The exothermic process in the second step, as expected, occurs in a wide temperature range (290–550 °C) and is due to the

Table 3 FT-IR assignments of ligand (H_2STCH) and their encapsulated complexes in cm^{-1}

Compound	Internal vibrations		External vibrations			$\nu_{(C=N)}$	$\nu_{(O-H)}$	$\nu_{(C-O)}$
	ν_{asym}T–O	ν_{sym}T–O	ν_{sym}T–O	ν_{asym}T–O	D–R			
H_2STCH	–	–	–	–	–	1596	3371	1266
[Mn(STCH)·$3H_2O$]-Y	1022	718	784	1119	578	1612	3420	1276
[Fe(STCH)·$3H_2O$]-Y	1018	733	775	1127	565	1619	3447	1273
[Co(STCH)·$3H_2O$]-Y	1025	725	760	1132	575	1625	3430	1270
[Ni(STCH)·$3H_2O$]-Y	1020	710	780	1122	560	1616	3440	1275
[Cu(STCH)·H_2O]-Y	1029	730	788	1125	572	1610	3426	1271

Table 4 Thermogravimetric analysis data of selected catalysts

Compound	Temperature range (°C)	Weight loss (%)	Group loss
[Mn(STCH)·3H_2O]-Y	40–260	16.6	Loss of intrazeolite + coordinated water molecules
	260–490	17.6	Loss of ligand
[Cu(STCH)·H_2O]-Y	40–290	14.9	Loss of intrazeolite + coordinated water molecules
	290–560	16.4	Loss of ligand

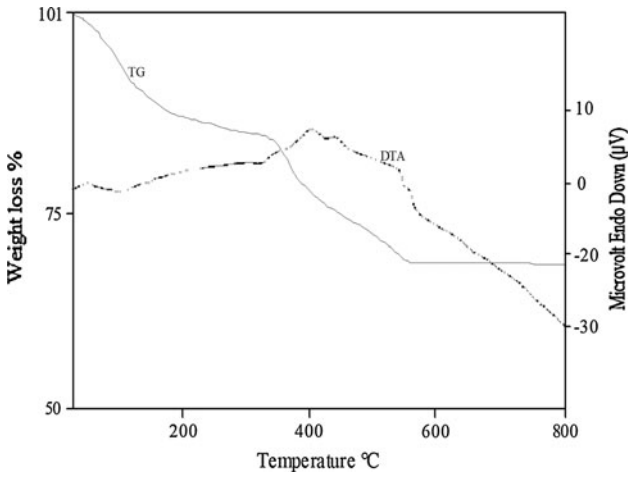

Fig. 3 TG and DTA thermogram of [Mn(STCH)·3H_2O]-Y

slow decomposition of the chelating ligand. A very small weight percentage loss (17.6%) indicates the presence of only small amount of metal complex insertion in the cavity of the zeolite-Y.

As a first step in our calculations, the constructed model structures for the ligand, and neat transition metal complexes were allowed to relax. This was done by using Broyden–Fletcher–Goldfarb–Shanno (BFGS) method. In the Mn(II) complex, the central metal has an octahedral environment, and the Cu(II) complex has the coordination number 4. The optimized structure of the [Mn(STCH)·3H_2O] type complex show a distorted octahedral geometry, made by the three water molecules, two oxygen and azomethine nitrogen of ligand, whereas in case of [Cu(STCH)·H_2O] show tetrahedrally distorted geometry along with one water molecule, two oxygen and azomethine nitrogen of ligand, which were summarized in Table 5 and Fig. 4. However, the [Mn(STCH)·3H_2O] structure has shown some distortion in the relaxed structure which were confirmed by the dihedral angles O(8)–N(9)–O(17)–Mn and O(20)–O(19)–O(21)–O(8) were 34.154 and 104.45° respectively. Further, the dihedral angle O(8)–O(19)–O(17)–N(9) and C(11)–C(12)–O(17)–Mn were 57.048 and 40.013° respectively, also confirmed a distortion of the Mn(II) complex. In the case of Cu(II) complex, only a very small distortion was observed for azomethine nitrogen of ligand; the dihedral angle C(11)–C(12)–N(9)–Cu was 65.006°.

The bond distance of Mn–O(19) is shorter than that of Cu–O(18), while Mn–N(9) distance is longer than Cu–O(9) complex, which might be due to the distorted octahedral Mn(II) complex. The calculated Mn–N(9) and Mn–O(20) bond length (∼2.0 Å) are consistent with the typical lengths in the octahedral coordinated Mn(II) complex, while the length of corresponding bonds for the tetrahedrally coordinated Cu(II) complexes are 1.6–1.7 Å [12]. Furthermore, the corresponding bond angles of the donor atoms of H_2STCH and Cu(II) ion are more acute for the tetrahedral geometry. The dihedral angles N(7)–C(6)–O(8)–Mn, O(20)–O(19)–O(8)–Mn and O(8)–N(9)–O(17)–Mn shows deviation from the regular octahedral geometry. The aperture of zeolite-Y is defined by a 12 member oxygen ring, having a larger cavity of diameter 12 Å and their unit is cubic (a = 24.7 Å), whereas the size of the neat Mn(II) and Cu(II) complexes are 12.043 and 12.039 Å respectively, smaller than the zeolite-Y cavity. This prevents complexes to come out of the zeolite cavity into the reaction medium.

The electronic density of states for ligand and transition metal complexes were presented in Fig. 5. It is clear that Cu(II) complex band structure were continuous valance and conduction bands, whereas Mn(II) has clearly more localized states in valence and conduction bands, which also confirms our prediction. Further, comparing the different DOS, we noticed that in the case of transition metal complex lead to a very small shift of the Fermi level towards higher energy. This can be explained by the electronic density of states of the ligand, which is free from transition metal. The HOMO–LUMO energy difference as presented in Table 6, for [Cu(STCH)·H_2O] is −4.164 eV which is more than −2.371 eV of [Mn(STCH)·3H_2O]. Similarly, the distortion of the metal complex upon encapsulation in various zeolites might change the position of HOMO and LUMO level of metal complexes.

Table 7 shows Fermi energy for ligand and neat complexes, is more for ligand and less in the case of Mn(II) complexes might be due to structural changes in relaxation. The shift in HOMO and LUMO energy difference from ligand H_2STCH may also due to the columbic effects,

Table 5 Selected distances, angles, and dihedral angles for neat complexes are calculated from relaxed structure

[Mn(STCH)·3H_2O]		[Cu(STCH)·H_2O]	
Distance (Å)			
Mn–O(19)	1.443	Cu–O(18)	1.745
Mn–N(9)	1.978	Cu–N(9)	1.450
Mn–O(21)	1.656	Cu–O(16)	2.438
Mn–O(8)	1.553	Cu–O(8)	1.657
Mn–O(20)	2.041		
Mn–O(17)	2.292		
Angle (°)			
O(20)–Mn–N(9)	53.214	O(16)–Cu–O(18)	123.355
O(20)–Mn–O(19)	101.003	O(16)–Cu–N(9)	80.341
O(19)–Mn–O(21)	67.200	O(18)–Cu–O(8)	109.081
O(21)–Mn–N(9)	104.147	N(9)–Cu–O(8)	101.332
O(19)–Mn–N(9)	171.012		
O(20)–Mn–O(21)	89.611		
O(17)–Mn–O(8)	108.080		
Dihedral angle (°)			
O(20)–O(19)–O(21)–O(8)	104.451	O(16)–O(18)–O(8)–N(9)	53.243
O(8)–O(19)–O(17)–N(9)	57.048	C(11)–C(12)–O(16)–Cu	10.528
C(11)–C(12)–O(17)–Mn	40.013	N(7)–C(6)–O(8)–Cu	4.421
N(7)–C(6)–O(8)–Mn	0.577	C(11)–C(10)–N(9)–Cu	65.006
O(20)–O(19)– O(8)–Mn	0.582	C(6)–N(7)–N(9)–Cu	57.698
O(8)–N(9)–O(17)–Mn	34.154		

coordination effects and vanderwaals interactions, whereas the columbic effects were produced by the charge distribution which might alter the energy level of metal complex shown in Table 7. The octahedral geometry for Mn(II) complex was also tested for the energy relaxation and found that Mn(II) octahedral is more stable than Cu(II) complex.

The catalytic hydroxylation of phenol was undertaken in a two-necked 50 mL round bottomed flask. In a typical reaction, 30 m mol of the substrate was taken in 2 mL of acetonitrile, add 45 mg of the catalyst to it and equilibrated at 80 °C in an oil-bath. 45 m mol of 30% H_2O_2 solution (phenol/H_2O_2 molar ratio, 1:1.5) was added to this with continuous stirring for 6 h and their results are given in Table 8. Blank experiments were performed without catalyst or with Na-Y zeolite show a lesser amount of % conversion. The products were collected at different time intervals and were identified and quantified by GC. The absence of metal ions in filtrate indicates that no leaching of complexes has occurred during reaction, as they are too intact in the nanopores [38].

Figure 6 summarizes the percentage conversion of phenol along with catechol and hydroquinone formations. It is clear from the results that the selectivity of catechol formation found to be varied (51–81%) from catalyst to catalyst. Interestingly all these catalysts are highly selective towards the catechol formation and the selectivity is maintained even after 24 h of reaction time. The conversion (%) of phenol increases in the order: [Cu(STCH)·H_2O]-Y > [Co(STCH)·3H_2O]-Y > [Fe(STCH)·3H_2O]-Y > [Ni(STCH)·3H_2O]-Y > [Mn(STCH)·3H_2O]-Y towards the formation of catechol selectively. In order to achieve suitable reaction conditions for the maximum hydroxylation, the parameters such as (I) Effect of solvent (II) Effect of amount of catalyst and (III) Effect of temperature were studied using [Cu(STCH)·H_2O]-Y as a representative catalyst. The results of these effects along with their possible explanations are summarized below:

The effect of various solvents over the hydroxylation of phenol with [Cu(STCH)·H_2O]-Y was studied. Five different solvents viz. chloroform, methanol, *n*-hexane, ethyl acetate and acetonitrile were taken to study their effect on the conversion. Though it is difficult to explain that which characteristic property of the solvent affects most to the % of phenol conversion, acetonitrile gives the best performance as the solvent (Fig. 7). The increasing order of % conversion can be given as: chloroform (9.5%) < methanol (20.1%) < *n*-hexane (32.8%) < ethyl acetate (38.5%) < acetonitrile (42.9%).

The amount of catalyst has a significant effect on the hydroxylation of phenol. Five different amounts of [Cu(STCH)·H_2O]-Y catalyst viz., 15, 25, 35, 45 and 50 mg

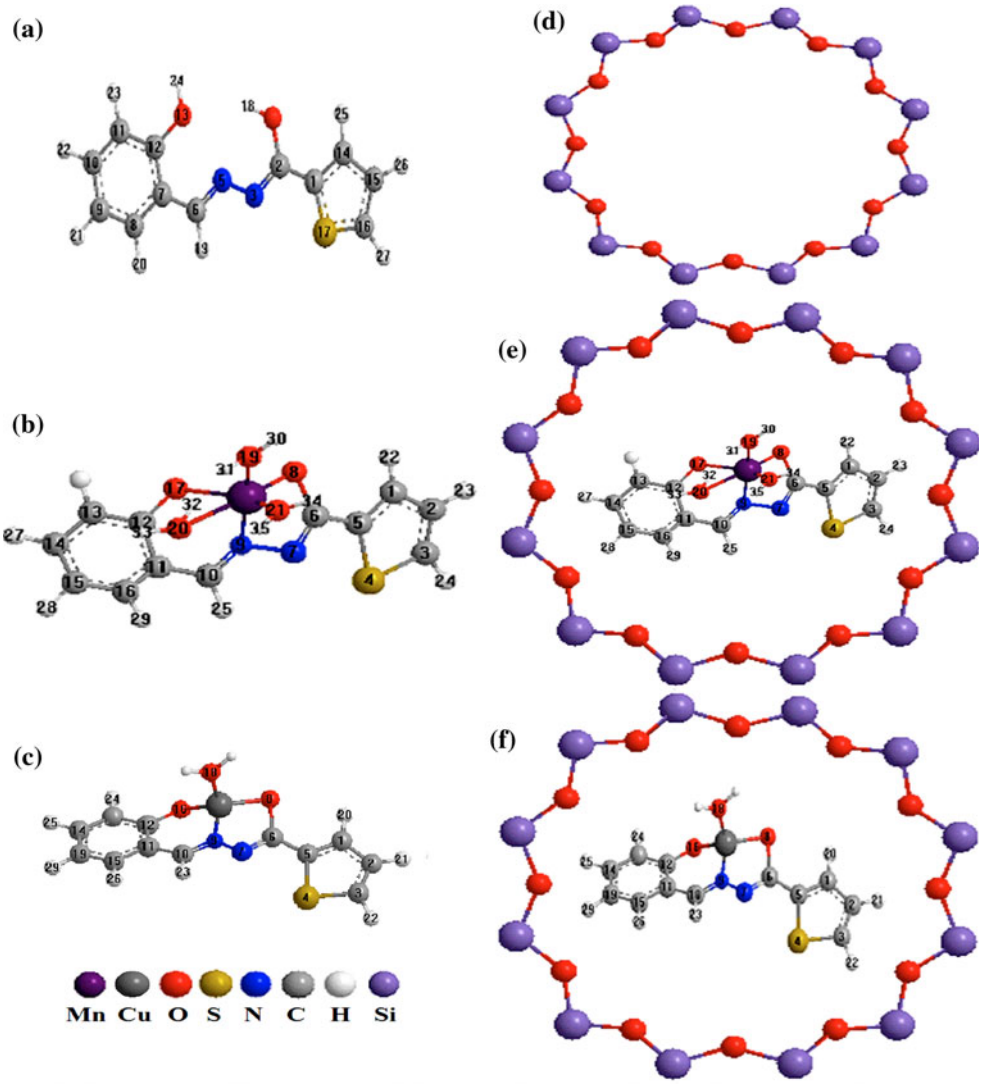

Fig. 4 Representative structures for H_2STCH ligand (**a**), neat distorted octahedral [Mn(STCH)·3H_2O] (**b**), tetrahedrally distorted [Cu(STCH)·H_2O] (**c**), zeolite-Y nanocavity (**d**), encapsulated [Mn(STCH)·3H_2O]-Y (**e**) and [Cu(STCH)·H_2O]-Y (**f**)

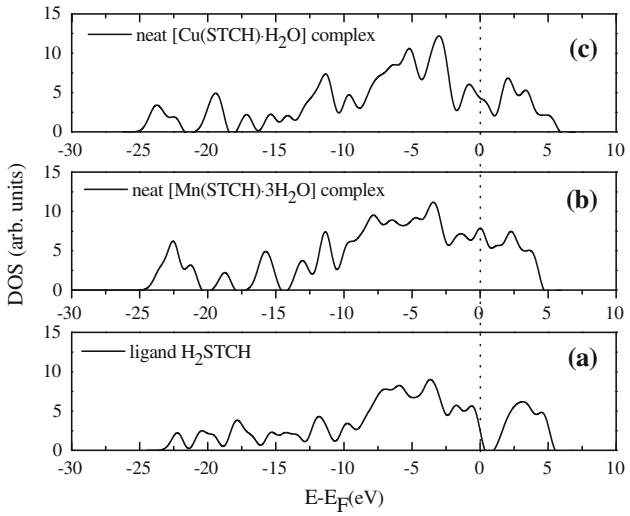

Fig. 5 Electronic density of states of ligand (**a**) and neat transition metal complexes (**b**, **c**), the Fermi level is set to be 0 eV

Table 6 The HOMO and LUMO energy difference (eV) for Schiff base ligand H_2STCH and neat complexes

Compound	HOMO–LUMO (eV)
H_2STCH	−2.011
[Mn(STCH)·3H_2O]	−2.371
[Cu(STCH)·H_2O]	−4.164

were used, keeping with all other reaction parameters fixed: namely temperature (80 °C), phenol (30 m mol), 30% H_2O_2 (45 m mol) in acetonitrile (2 mL) and reaction time (6 h). The results are shown in Fig. 8, indicating 30.5, 33.7, 39.8, 42.9 and 42.9% conversion corresponding to 15, 25, 35, 45 and 50 mg catalyst, respectively. Lower conversion of phenol with 15 and 25 mg catalyst may be due to fewer catalytic sites. The greater conversion percentage was observed with 45 mg catalyst but there was no remarkable

Table 7 Relaxed parameters of ligand and neat metal complexes using density functional calculation

Compound	Total energy (eV)[a]	Fermi energy (eV)	One electron contribution (eV)	Ewald contribution (eV)
H_2STCH	−3696.266	3.572	−2662.567	−1765.770
[Mn(STCH)·3H_2O]	−7901.203	2.472	−7889.336	−2809.541
[Cu(STCH)·H_2O]	−5776.925	3.351	−3429.296	−3001.547

[a] Harris-Foulkes estimate

Table 8 Hydroxylation of phenol to catechol and hydroquinone with 30% H_2O_2 catalyzed by encapsulated complexes (temperature 80 °C; phenol/H_2O_2 molar ratio, 1:1.5; time, 6 h; catalyst, 45 mg)

Sr. no.	Compound	Conversion (%)	Selectivity (%)	
			Catechol	Hydroquinone
1	[Mn(STCH)·3H_2O]-Y	17.7	57.8	42.2
2	[Fe(STCH)·3H_2O]-Y	27.9	72.9	27.1
3	[Co(STCH)v3H_2O]-Y	34.1	77.5	22.5
4	[Ni(STCH)·3H_2O]-Y	21.2	63.7	36.3
5	[Cu(STCH)·H_2O]-Y	42.9	81.3	18.7
6	[Cu(STCH)·H_2O]-Y[a]	41.6	80.2	19.8
7	[Cu(STCH)·H_2O]-Y[b]	38.8	78.9	21.1
8	Cu^{II}-Y	16.3	51.4	48.6

[a] First reuse

[b] Second reuse

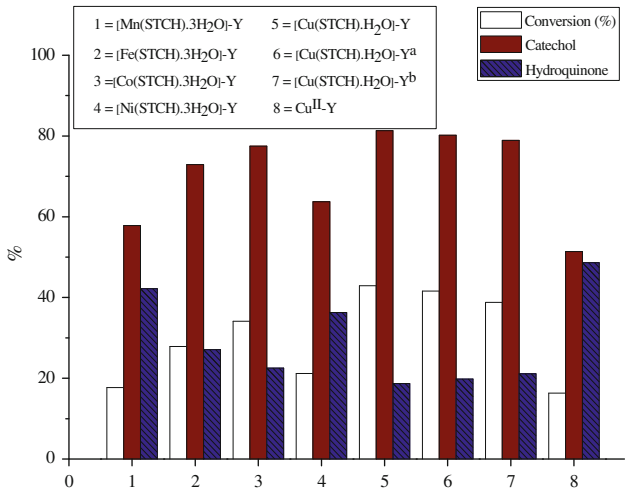

Fig. 6 Conversion % of phenol hydroxylation

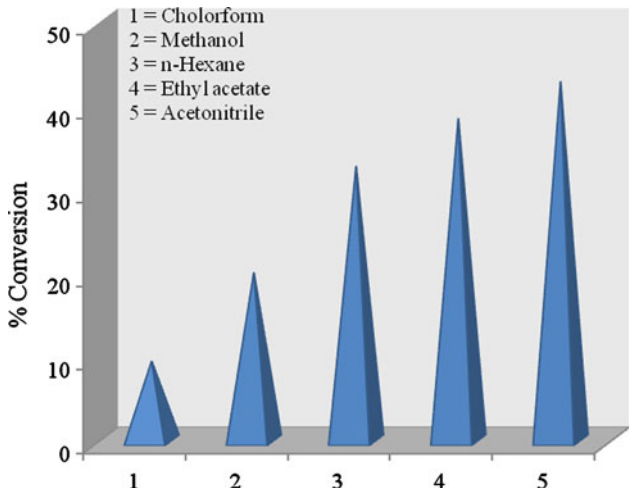

Fig. 7 Effect of solvent on the hydroxylation of phenol

difference in the progress of reaction when more than 45 mg of catalyst was employed. Therefore, 45 mg amount of catalyst was taken to be optimal.

Similarly, for four different temperatures viz. 60, 70, 75, and 80 °C, the effect of temperature on the hydroxylation of phenol (Fig. 9) was examined at under the above reaction conditions, phenol (30 m mol), 30% H_2O_2 (45 m mol), catalyst (45 mg) in acetonitrile (2 mL) for 6 h. The result reveals that on increasing the temperature from 60 to 80 °C, the improvements was observed and further no change in % conversion of hydroxylation of phenol. Consequently at 80 °C for 6 h time is considered to be the optimum.

The representative catalyst [Cu(STCH)·H_2O]-Y was recycled for the oxidation of phenol with a view to establish the effect of encapsulation on stability. The initial run shows a conversion of 42.9% and it just marginally reduced to 41.6 and 38.8% after first and second recycling the catalyst, respectively. These results indicate that [Cu(STCH)·H_2O]-Y catalyst is almost stable to be recycled for the oxidation of phenol without much loss in activity. Consequently, the encapsulation of metal complexes inside the nanocavity of zeolite-Y is found to increase the life of catalyst by reducing

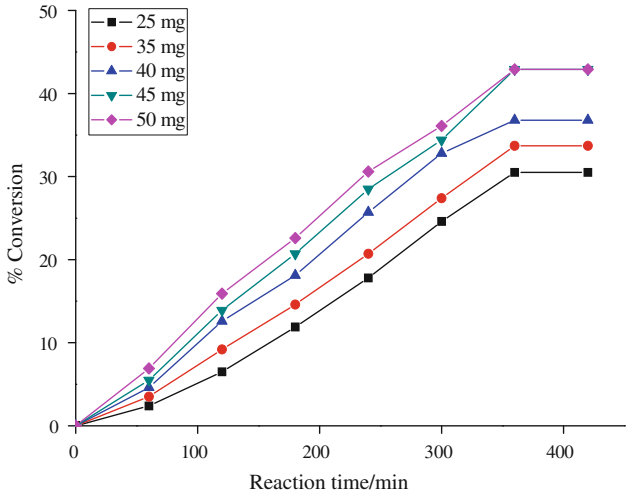

Fig. 8 Effect of amount of catalyst on the hydroxylation of phenol

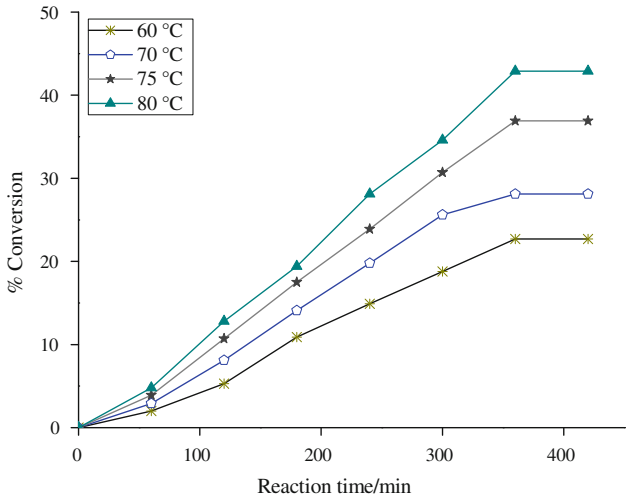

Fig. 9 Effect of temperature on the hydroxylation of phenol

dimerization due to restriction of internal framework structure.

Concluding remarks

In summary, a series of zeolite-encapsulated hybrid catalysts have been prepared by FLM, as evidenced by ICP-OES, elemental analyses, spectral studies, BET, SEMs, X-ray diffraction patterns and TG–DTA studies. Furthermore, the spectroscopic data suggest that the crystallinity of the zeolite has not undergone any significant change during the process of encapsulation. HOMO and LUMO energy difference gap were calculated from first-principles. The relaxed total energy indicates that Mn(II) is more stable than that of Cu(II) complexes. The encapsulated hybrid materials exhibit catalytic activity for the hydroxylation of phenol using hydrogen peroxide affording catechol and hydroquinone, with good catechol selectivity in the order: [Cu(STCH)·H_2O]-Y > [Co(STCH)·$3H_2O$]-Y > [Fe(STCH)·$3H_2O$]-Y > [Ni(STCH)·$3H_2O$]-Y > [Mn(STCH)·$3H_2O$]-Y. This shows that [Cu(STCH)·H_2O]-Y catalyst has the highest % of catechol selectivity (81.3%).

Acknowledgments We express our gratitude to the Head, Department of Chemistry, Bhavnagar University, Bhavnagar, India for providing the necessary laboratory facilities. Mr. Parthiv M. Trivedi would like to acknowledge UGC, Delhi for providing meritorious fellowship. One of us (SKG) is indebted to the Ministry of New and Renewable Energy (MNRE) for awarding the post-doc fellowship. An analytical facility provided by the IIT Bombay, CSMCRI, Bhavnagar and Computations were carried out on the computer cluster PAWAN at the Department of Physics, Bhavnagar University financed by the Department of Science and Technology, Govt. of India.

References

1. Maurya, M.R., Chandrakar, A.K., Chand, S.: Oxidation of phenol, styrene and methyl phenyl sulfide with H_2O_2 catalysed by dioxovanadium(V) and copper(II) complexes of 2-aminomethylbenzimidazole-based ligand encapsulated in zeolite-Y. J. Mol. Catal. A: Chem **263**, 227–237 (2007)
2. Salavati-Niasari, M., Bazarganipour, M.: Host (nanodimensional pores of zeolite Y)-guest (tetraaza[14]annulene nickel(II) complexes, [Ni(Me_4R_2Bzo[14]tetraeneN_4)]) nanocomposite materials: ship-in-a-bottle synthesis, characterization and liquid phase oxidation of phenol with hydrogen peroxide. Catal. Commun. **7**, 336–343 (2006)
3. Salavati-Niasari, M.: Synthesis, characterization of cobalt(II) complex nanoparticles encapsulated within nanoreactors of zeolite-Y and their catalytic activities. J. Mol. Catal. A: Chem. **310**, 51–58 (2009)
4. Salavati-Niasari, M., Davar, F.: Synthesis, characterization, and catalytic oxidation of ethylbenzene over host (zeolite-Y)/guest (copper(II) complexes of tetraaza macrocyclic ligands) nanocomposite materials. J. Coord. Chem. **63**, 3240–3255 (2010)
5. Bansal, V.K., Thankachan, P.P., Prasad, R.: Oxidation of benzyl alcohol and styrene using H_2O_2 catalyzed by tetraazamacrocycle complexes of Cu(II) and Ni(II) encapsulated in zeolite-Y. Appl. Catal. A: Gen **381**, 8–17 (2010)
6. Abbo, H.S., Titinchi, S.J.J.: Di-, tri- and tetra-valent ion-exchanged NaY zeolite: active heterogeneous catalysts for hydroxylation of benzene and phenol. Appl. Catal. A: Gen **356**, 167–171 (2009)
7. Farzaneh, F., Poorkhosravania, M., Ghandi, M.: Utilization of immobilized biomimetic iron complexes within nanoreactors of Al-MCM-41 as cyclohexane oxidation catalyst. J. Mol. Catal. A: Chem **308**, 108–113 (2009)
8. Nunes, N., Amaro, R., Costa, F., Rombi, E., Carvalho, A.M., Neves, I.C., Fonseca, A.M.: Copper(II)-purine complexes encapsulated in NaY zeolite. Eur. J. Inorg. Chem. **2007**, 1682–1689 (2007)
9. Notari, B.: Chemistry of microporous crystals. In: Inui, T., Namba, S., Tatsumi, T. (eds.) Studies in surface science and catalysis. Elsevier, Amsterdam (1991)
10. Reddy, J.S., Sivasanker, S., Ratnasamy, P.: Hydroxylation of phenol over TS-2, a titanium silicate molecular sieve. J. Mol. Catal. **71**, 373–381 (1992)
11. Maurya, M.R., Kumar, M., Kumar, A., Costa Pessoa, J.: Oxidation of p-chlorotoluene and cyclohexene catalysed by polymer-

anchored oxovanadium(IV) and copper(II) complexes of amino acid derived tridentate ligands. Dalt. Trans. **263**, 4220–4232 (2008)
12. Biernacka, I.K., Biernacka, K., Magalhães, A.L., Fonseca, A.M., Neves, I.C.: Catalytic behavior of 1-(2-pyridylazo)-2-naphthol transition metal complexes encapsulated in Y zeolite. J. Catal. **278**, 102–110 (2011)
13. Ganesan, R., Vishwanathan, B.: Redox properties of bis(8-hydroxyquinoline) manganese(II) encapsulated in various zeolites. J. Mol. Catal. A: Chem **223**, 21–29 (2004)
14. Sawabe, K., Hiro, T., Shimizu, K.-I., Satsuma, A.: Density functional theory calculation on the promotion effect of H_2 in the selective catalytic reduction of NO_x over Ag-MFI zeolite. Catal. Today **153**, 90–94 (2010)
15. Gotsev, M.G., Ivanov, P.M.: Molecular dynamics of large-ring cyclodextrins: principal component analysis of the conformational interconversions. J. Phys. Chem. B **113**, 5752–5759 (2009)
16. Zhou, H.W., Lai, W.P., Zhang, Z.Q., Li, W.K., Cheung, H.Y.: Computational study on the molecular inclusion of andrographolide by cyclodextrin. J. Comput. Aided Mol. Des. **23**, 153–162 (2009)
17. Anconi, C.P.A., Nascimento Jr., C.S., Fedoce-Lopes, J., Santos, H.F.D., Almeida, W.B.D.: Ab initio calculations on low-energy conformers of α-cyclodextrin. J. Phys. Chem. A **111**, 12127–12135 (2007)
18. Pan, Y.-X., Liu, C.-J., Ge, Q.: Effect of surface hydroxyls on selective CO_2 hydrogenation over Ni_4/γ-Al_2O_3: A density functional theory study. J. Catal. **272**, 227–234 (2010)
19. Rybakov, A.A., Larin, A.V., Zhidomirov, G.M., Trubnikov, D.N., Vercauteren, D.P.: DFT investigation of CO oxidation over Mg exchanged periodic zeolite models. Comput. Theo. Chem. **964**, 108–115 (2011)
20. Yin, H.D., Chen, S.W., Li, L.W., Qi, D.: Synthesis, characterization and crystal structures of the organotin(IV) compounds with the Schiff base ligands of pyruvic acid thiophene-2-carboxylic hydrazone and salicylaldehyde thiophene-2-carboxylic hydrazone. Inorg. Chim. Acta **360**, 2215–2223 (2007)
21. Hohenberg, P., Kohn, W.: Inhomogeneous electron gas. Phys. Rev. **136**, B864–B871 (1964)
22. Kohn, W., Sham, L.J.: Self-consistent equations including exchange and correlation effects. Phys. Rev. **140**, A1133–A1138 (1965)
23. Baroni, S., Corso, A.D., de Gironcoli, S., Giannozzi, P. <http://www.pwscf.org>
24. Baroni, S., Gironcoli, S., De, A., Dal, C., Giannozzi, P.: Phonons and related crystal properties from density-functional perturbation theory. Rev. Mod. Phys. **73**, 515–562 (2001)
25. Perdew, J.P., Burke, K., Ernzerhof, M.: Generalized gradient approximation made simple. Phys. Rev. Lett. **77**, 3865–3868 (1996)
26. Monkhorst, H.J., Pack, J.D.: Special points for brillouin-zone integrations. Phys. Rev. B **13**, 5188–5192 (1976)
27. Marzari, N., Vanderbilt, D., Payne, M.C.: Ensemble density-functional theory for ab initio molecular dynamics of metals and finite-temperature insulators. Phys. Rev. Lett. **79**, 1337–1340 (1997)
28. Dutta, B., Jana, S., Bera, R., Saha, P.K., Koner, S.: Immobilization of copper Schiff base complexes in zeolite matrix: preparation, characterization and catalytic study. Appl. Catal. A: Gen **318**, 89–94 (2007)
29. Chen, P., Fan, B., Song, M., Jin, C., Ma, J., Li, R.: Zeolite-encapsulated Ru(III) tetrahydro-Schiff base complex: an efficient heterogeneous catalyst for the hydrogenation of benzene under mild conditions. Catal. Commun. **7**, 969–973 (2006)
30. Modi, C.K., Jani, D.H., Patel, H.S., Pandya, H.M.: Novel Fe(III) heterochelates: synthesis, structural features and fluorescence studies. Spectrochim. Acta A **75**, 1321–1328 (2010)
31. Modi, C.K., Jani, D.H.: Novel Mn(III) heterochelates: synthesis, thermal, spectroscopic, and coordination aspects. J. Therm. Anal. Calorim. **102**, 1001–1010 (2010)
32. Nakamoto, K.: Infrared spectra and Raman spectra of inorganic and coordination compounds, part B: application in coordination, organometallic, and bioinorganic chemistry, 6th edn. Wiley Interscience, New Jersey (2009)
33. Ahmed, A.H., Mostafa, A.G.: Synthesis and identification of zeolite-encapsulated iron(II), iron(III)-hydrazone complexes. Mater. Sci. Eng. C **29**, 877–883 (2009)
34. Modi, C.K.: Synthesis, spectral investigation and thermal aspects of coordination polymeric chain assemblies of some transition metal ions with bis-pyrazolones. Spectrochim. Acta A **71**, 1741–1748 (2009)
35. El-Metwaly, N.M.: Spectral and biological investigation of 5-hydroxyl-3-oxopyrazoline 1-carbothiohydrazide and its transition metal complexes. Trans. Met. Chem. **32**, 88–94 (2007)
36. Maki, A.H., McGarvey, B.R.: Electron spin resonance in transition metal chelates. II. copper(II) bis-salicylaldehyde-imine. J. Chem. Phys. **29**, 35–38 (1958)
37. Modi, C.K., Patel, I.A., Thaker, B.T.: Manganese(III) schiff-base complexes involving heterocyclic β-diketone and diethylene triamine. J. Coord. Chem. **61**, 3110–3121 (2008)
38. Ghandi, M., Alizadeh, M.: Immobilized copper(II) complexes on montmorillonite and MCM-41 as selective catalysts for epoxidation of alkenes. J. Mol. Catal. A: Chem **233**, 127–131 (2005)